

Long-span suspension bridge flutter analysis with drag force effects

Original

Long-span suspension bridge flutter analysis with drag force effects / Piana, G.; Carpinteri, A.. - In: JOURNAL OF APPLIED AND COMPUTATIONAL MECHANICS. - ISSN 2383-4536. - STAMPA. - 7:SI(2021), pp. 1077-1089. [10.22055/JACM.2021.32481.2025]

Availability:

This version is available at: 11583/2913780 since: 2021-07-19T15:49:04Z

Publisher:

Shahid Chamran University

Published

DOI:10.22055/JACM.2021.32481.2025

Terms of use:

This article is made available under terms and conditions as specified in the corresponding bibliographic description in the repository

Publisher copyright

(Article begins on next page)



Journal of Applied and Computational Mechanics



Research Paper

Long-span Suspension Bridge Flutter Analysis with Drag Force Effects

Gianfranco Piana^{1,2}, Alberto Carpinteri^{3,4}

¹ Politecnico di Torino, Department of Structural, Geotechnical and Building Engineering, Corso Duca degli Abruzzi 24, Torino, 10129, Italy, Email: gianfranco.piana@polito.it

² Tongji University, Department of Bridge Engineering, 1239 Siping Road, Shanghai, 200092, P. R. China

³ Politecnico di Torino, Department of Structural, Geotechnical and Building Engineering, Corso Duca degli Abruzzi 24, Torino, 10129, Italy, Email: alberto.carpinteri@polito.it

⁴ Shantou University, Department of Civil and Environmental Engineering, Shantou, Guangdong, 515063, P. R. China

Received February 01 2020; Revised April 29 2021; Accepted for publication May 22 2021.

Corresponding author: G. Piana (gianfranco.piana@polito.it)

© 2021 Published by Shahid Chamran University of Ahvaz

Abstract. The paper investigates the influence of the drag force onto the flutter velocity and frequency of the Akashi Kaikyo Bridge. Finite element analyses were run in ANSYS by combining unsteady lift and moment actions with: (a) unsteady drag, (b) steady drag, (c) no drag. The finite element results are compared to those obtained by an *in-house* MATLAB code based on a semi-analytic continuum model and with others from the literature. The continuum model includes flexural-torsional second-order effects induced by steady drag force into the bridge's equations of motion, in addition to unsteady lift and moment actions. The results show that good predictions of the flutter velocity can be obtained by combining steady drag with unsteady lift and moment.

Keywords: Aeroelastic Flutter, Suspension Bridge, Akashi Kaikyo Bridge, Finite Element Model, Semi-analytic Model, Drag Force.

1. Introduction

As is well known since the famous Tacoma Narrows Bridge collapse of November 7th, 1940, flutter is the most dangerous aeroelastic phenomenon concerning the design against wind of long-span cable-supported bridges [1]. In fact, wind represents the actual "design action" for flexible bridge schemes like those employed to range long distances [2]. In practice, bridge flutter analysis basically rests on the theory proposed by Scanlan and Tomko in 1971 [3], and later refined by Scanlan himself and by other researchers [4]-[6]. Such theory transposes the theory of wing flutter to bridge decks, where in the latter case the unsteady aerodynamic loads related to the bridge deck's harmonic motion are expressed in terms of parameters (the so-called aeroelastic or flutter derivatives) that are experimentally determined in the wind tunnel rather than analytically computed. The theory is supposed to be valid only for small displacements and rotations and for laminar incident flow, but it is commonly used to define the onset of aeroelastic instability in real cases. Recent advancements have been proposed that use aeroelastic derivatives to perform nonlinear flutter analyses [7]. *Ad hoc* numerical procedures have been developed to analyze full bridge flutter in a finite element framework, both in the frequency and time domains (e.g. see [8-10]). The literature on the subject is very vast and in continuous expansion; here we only refer to some of the fundamental studies and to those papers that are, in some way, directly connected to the presents work. An interesting historical view of long-span bridge aerodynamics is given in [11], whereas a wide review of methods for flutter stability analysis of long-span bridges can be found in [12].

Flutter stability analysis of long-span bridges is usually conducted as a damped complex eigenvalue analysis, where the aeroelastic (self-excited or motion-dependent) forces acting on the bridge deck are expressed as linear functions of deck's displacements and velocities [5]. In most practical applications, among the general three aeroelastic forces of drag, lift, and pitching moment, only the latter two are of interest, the former being of little importance for dynamic stability. However, both numerical (FEM) calculations and wind tunnel tests conducted before the construction of the Akashi Kaikyo Bridge – current world record with its central span of 1991 m – showed that all the three aeroelastic components of lift, drag and moment are of interest for spans above around 1.5 km [13]. According to the most general formulation, eighteen flutter derivatives are required for a complete description [5,14]. Their evaluation in the wind tunnel is a hard and expensive task; fortunately, some of them are less important than others, and studies that provide reliable, simplified approaches are of interest, especially for their practical usefulness in early and intermediate design stages [15].

The present work aimed at investigating the role played by the description of the drag component on the predicted flutter velocity, and frequency, of very long-span suspension bridges. The Akashi Kaikyo Bridge was selected as a benchmark. To the purpose, a detailed finite element model of the central span of the bridge was implemented in ANSYS. The user-defined Matrix27 element [16-18] was incorporated into the model to define the nodal aeroelastic forces by means of element aerodynamic stiffness and damping matrices. Flutter analyses were thus run considering the following descriptions of the wind aerodynamic actions:



- 1) Unsteady (motion-dependent) lift, moment, and drag;
- 2) Unsteady lift and moment plus steady (motion-independent) drag;
- 3) Unsteady lift and moment with no drag.

The finite element results were compared to those obtained by an *in-house* MATLAB code based on a semi-analytic continuum model. The latter includes flexural-torsional second-order effects induced by steady drag force into the bridge equations of motion, in addition to unsteady lift and moment actions. Reference to literature results was also done for further comparisons. The present paper extends and enhances a previous conference paper by the authors [19], dealing with the same problem. In that study, the results provided by the semi-analytic model were satisfactory in terms of flutter speed, but less good in terms of flutter frequency. Thus, a preliminary free-dynamics analysis with no wind was added in this study to set the parameters and the boundary conditions of the continuum model prior to the flutter analysis. The results in terms of natural vibration frequencies and mode shapes of the bridge are presented in this paper together with those of the new flutter analysis, showing a better match in terms of both flutter speed and frequency. In addition, more details are also provided here about the adopted procedures, as well as new comparisons with literature results and possible further developments.

2. Aerodynamic Actions and Flutter Analysis Methods

2.1 Aerodynamic loading models

With reference to a deck-girder section model with at most three degrees of freedom in the plane, linearly damped and elastically supported, the following three descriptions of the aerodynamic actions produced by a laminar transverse wind were adopted in this study:

- Case 1)

$$L_{se} = \frac{1}{2} \rho U^2 B \left(KH_1^* \frac{\dot{h}}{U} + KH_2^* \frac{B\dot{\alpha}}{U} + K^2 H_3^* \alpha + K^2 H_4^* \frac{h}{B} + KH_5^* \frac{\dot{p}}{U} + K^2 H_6^* \frac{p}{B} \right), \quad (1)$$

$$D_{se} = \frac{1}{2} \rho U^2 B \left(KP_1^* \frac{\dot{p}}{U} + KP_2^* \frac{B\dot{\alpha}}{U} + K^2 P_3^* \alpha + K^2 P_4^* \frac{p}{B} + KP_5^* \frac{\dot{h}}{U} + K^2 P_6^* \frac{h}{B} \right), \quad (2)$$

$$M_{se} = \frac{1}{2} \rho U^2 B^2 \left(KA_1^* \frac{\dot{h}}{U} + KA_2^* \frac{B\dot{\alpha}}{U} + K^2 A_3^* \alpha + K^2 A_4^* \frac{h}{B} + KA_5^* \frac{\dot{p}}{U} + K^2 A_6^* \frac{p}{B} \right), \quad (3)$$

where: L_{se} , D_{se} , M_{se} are the unsteady (self-excited) aerodynamic actions of lift, drag, and moment per unit length, respectively; ρ is the air mass density; U is the wind speed; B is the deck width; $K = \omega B/U$ is the reduced circular frequency (ω is the circular frequency); h , p , α are the vertical (heaving), lateral (sway), torsional generalized displacements, respectively (dotted symbols represent time derivatives); H_i^* , P_i^* , A_i^* ($i=1, 2, \dots, 6$) are the non-dimensional flutter derivatives, which are functions of K . They are usually evaluated in the wind tunnel for the deck section of interest, and plotted as functions of the reduced velocity $U_r = 2\pi/K$ [19],[21].

- Case 2)

Lift and moment were assumed as self-excited forces according to Eqs. (1) and (3), respectively, whereas the drag force was assumed as a steady force, evaluated for zero attack angle, as follows:

$$D_s := D_s(0) = \frac{1}{2} \rho U^2 B C_D(0), \quad (4)$$

where $C_D(0)$ is the steady drag coefficient, which is a function of the deck section and wind attack angle α , evaluated for zero angle of attack (the notation (0) refers to the angle of attack $\alpha=0^\circ$) [19],[21].

- Case 3)

Lift and moment were assumed as self-excited forces according to Eqs. (1) and (3) as in the previous cases, whereas the drag force was neglected.

2.2 Finite element flutter analysis

The finite element setting for linear flutter analysis writes as follows:

$$\mathbf{M}\ddot{\mathbf{X}} + (\mathbf{C} - \mathbf{C}_{ae})\dot{\mathbf{X}} + (\mathbf{K} - \mathbf{K}_{ae})\mathbf{X} = \mathbf{0}, \quad (5)$$

where: \mathbf{M} , \mathbf{C} , \mathbf{K} are the global mass, damping, and stiffness matrices, \mathbf{C}_{ae} , \mathbf{K}_{ae} are the aerodynamic damping and stiffness matrices, respectively, all obtained by assembly of the corresponding local (element) matrices; \mathbf{X} is the dynamic response vector. \mathbf{C}_{ae} , \mathbf{K}_{ae} are evaluated based on the aerodynamic loading descriptions in Section 2.1, adopting a lumped formulation.

When using the lumped formulation, the element aerodynamic stiffness and damping matrices are:

$$\mathbf{K}_{ae}^e = \begin{bmatrix} \mathbf{K}_{ae1}^e & 0 \\ 0 & \mathbf{K}_{ae1}^e \end{bmatrix}, \quad \mathbf{C}_{ae}^e = \begin{bmatrix} \mathbf{C}_{ae1}^e & 0 \\ 0 & \mathbf{C}_{ae1}^e \end{bmatrix}, \quad (6a, b)$$



$$\mathbf{K}_{ae1}^e = a_0 \begin{bmatrix} 0 & 0 & 0 & 0 & 0 & 0 \\ 0 & P_6^* & P_4^* & BP_3^* & 0 & 0 \\ 0 & H_6^* & H_4^* & BH_3^* & 0 & 0 \\ 0 & BA_6^* & BA_4^* & B^2A_3^* & 0 & 0 \\ 0 & 0 & 0 & 0 & 0 & 0 \\ 0 & 0 & 0 & 0 & 0 & 0 \end{bmatrix}, \quad \mathbf{C}_{ae1}^e = b_0 \begin{bmatrix} 0 & 0 & 0 & 0 & 0 & 0 \\ 0 & P_5^* & P_1^* & BP_2^* & 0 & 0 \\ 0 & H_5^* & H_1^* & BH_2^* & 0 & 0 \\ 0 & BA_5^* & BA_1^* & B^2A_2^* & 0 & 0 \\ 0 & 0 & 0 & 0 & 0 & 0 \\ 0 & 0 & 0 & 0 & 0 & 0 \end{bmatrix}, \quad (7a, b)$$

where $a_0 = \rho U^2 K^2 L_e / 2$, $b_0 = \rho UBKL_e / 2$; L_e is the length of element e .

Matrices \mathbf{K}_{ae}^e and \mathbf{C}_{ae}^e in Eqs. (6a, b) and (7a, b) are the same for each element of the bridge model, according to a usually adopted approximation. In fact, the aerodynamic derivatives H_i^* , P_i^* , and A_i^* are obtained from sectional models that have two-dimensional characteristics (assumption of bi-dimensional flow), so that three-dimensional features of the aerodynamic flow are neglected. In other words, the aerodynamic stiffness and damping are assumed constant along the bridge deck. On the other hand, a spatial variation of the wind force along the bridge axis can easily be introduced via a multiplicative function affecting the wind speed U (wind spatial distribution coefficient), but this is often not done since assuming a uniform wind distribution is conservative, and thus on the safe side. In addition, studies have proven the effect of turbulence – not included in this formulation – to be beneficial against flutter (i.e., increases the stability limit), and therefore its contribution is usually ignored [19].

By Eq. (5), a damped complex eigenvalue analysis can be carried out to study the dynamic stability of the discretized bridge structure for increasing wind speeds. The dynamic response can be approximated by a superposition of the first m conjugate pairs of complex eigenvalues and eigenvectors, as:

$$\mathbf{X} = \sum_{j=1}^m \mathbf{x}_j e^{\lambda_j t}, \quad (8)$$

where $\mathbf{x}_j = \mathbf{p}_j \pm i\mathbf{q}_j$ is the j^{th} complex conjugate pair of eigenvectors, $\lambda_j = \sigma_j \pm i\omega_j$ is the j^{th} complex eigenvalue.

The system is dynamically stable if the real part of all eigenvalues is negative and dynamically unstable if the real part of one or more eigenvalues is positive. The condition for occurrence of flutter instability is then identified as follows: for certain wind velocity U_f the system has one complex eigenvalue λ_f with zero or near zero real part, the corresponding wind velocity U_f being the critical flutter wind velocity and the imaginary part of the complex eigenvalue λ_f becoming the flutter frequency. A mode-by-mode tracing method must be employed to iteratively search for the flutter frequency and determine the critical flutter wind velocity.

According to the analysis method proposed in [16], the element aerodynamic stiffness and damping matrices can be built-up in ANSYS by a specific user-defined Matrix27 element. Such element can only model either an aerodynamic stiffness matrix or an aerodynamic damping matrix, therefore a pair of Matrix27 elements must be attached to each node of a generic bridge deck element. Matrix 27 elements represent fictitious finite elements that can conveniently be introduced into the geometry to obtain a hybrid finite element model of the bridge suitable to perform a flutter analysis in ANSYS [16]. In the analyses conducted in the present study, the aerodynamic actions (both self-excited and steady) were neglected for the suspension cables.

2.3 Semi-analytic continuum model for flutter analysis with drag-induced second-order effects

With reference to the single-span suspension bridge scheme in Fig. 1, the structure is composed of a deck-girder, modeled as an elastic beam of constant cross-section, deformable in flexure and torsion, inextensible and not deformable in shear, vertically suspended to the main cables by a continuous system of hangers. The main cables are modeled as tension-only elastic elements. The hangers are modeled as inextensible bars. The deck-girder is simply supported at the ends for both vertical bending and torsion, and is supposed to be straight under permanent loads. The pair of main suspending cables, having shallow parabolic profile (sag-to-span ratio < 1/8), is connected to fixed points with same height. A reduced elastic modulus of the cables is introduced to suitably take into account the compliance of the end portions of the cables between towers and anchorages.

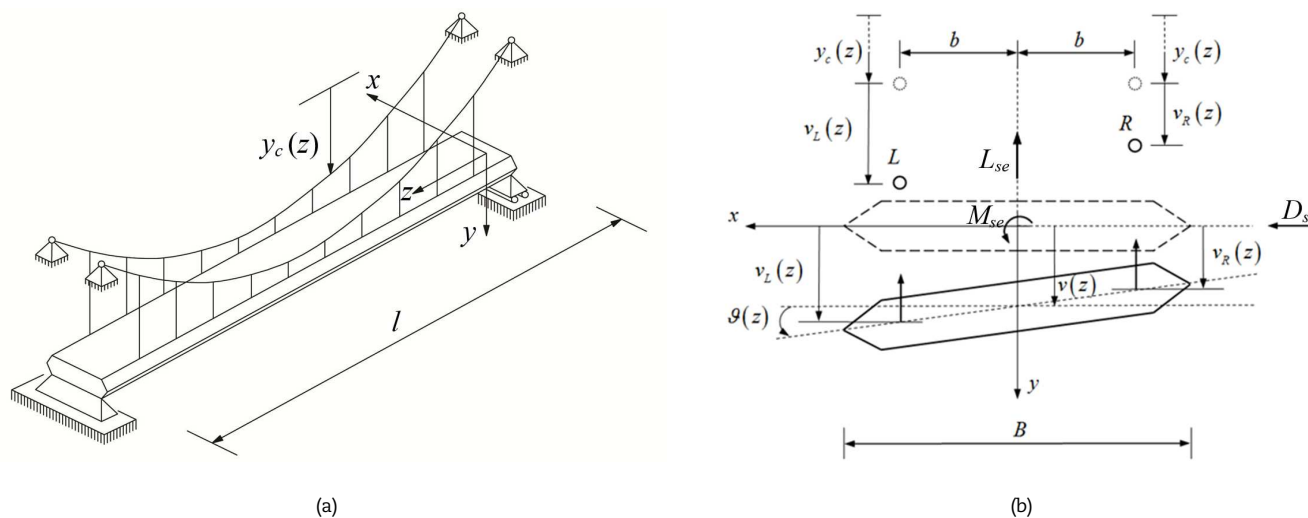


Fig. 1. Single-span suspension bridge model: (a) static scheme and (b) cross-section before and after bending-torsion deformation.



According to the previous assumptions, under the action of uniformly distributed steady drag force and unsteady lift and moment, the equations of motion of the deck-girder, described in terms of vertical deflection, $v(z,t)$, and torsion rotation of the beam sections, $\vartheta(z,t)$, where z is the abscissa measured along the beam centroidal axis and t is time, write:

$$E_1(z,t) := \mu_g \ddot{v} + c_v \dot{v} + EI_x v'''' - H v'' + (m_y \vartheta)'' - y_c''(h_R(t) + h_L(t)) - L_{se} = 0, \tag{9a}$$

$$E_2(z,t) := I_\vartheta \ddot{\vartheta} + c_\vartheta \dot{\vartheta} + EI_\omega \vartheta'''' - (GI_t + Hb^2) \vartheta'' + m_y v'' + b y_c''(h_R(t) - h_L(t)) - M_{se} = 0, \tag{9b}$$

where: μ_g, I_g , are the bridge's (deck-girder, cables and hangers) mass, polar mass moment of inertia per unit length; $c_v=2\mu_g\zeta_v\omega_v$, $c_\vartheta=2I_\vartheta\zeta_\vartheta\omega_\vartheta$ are the damping coefficients (with ζ_v, ζ_ϑ the damping ratios, $\omega_v, \omega_\vartheta$ the angular frequencies); EI_x is the bending rigidity in the vertical plane (x is the cross-section horizontal axis through the centroid); EI_ω, GI_t are the warping (Vlasov), primary (St. Venant) torsion rigidities; H is the total horizontal component of the main cables tension due to the bridge weight per unit length, q_g ($H=q_g l^2/8f$, with l the bridge (central) span and f the cables sag); m_y is the bending moment in the horizontal plane, due to the steady drag, D_s , given by Eq. (4) (y is the cross-section vertical axis through the centroid; y_c is the initial profile of the main cables, assumed parabolic. Overdots denote differentiation with respect to time t , apices denote differentiation with respect to z . h_R, h_L are the additional horizontal components of the right, left cable tensions (nil for antisymmetric deformations), given by [22]:

$$h_R(t) = \frac{E_c(A_c/2)q_g}{L} \int_0^l (v(z,t) - b\vartheta(z,t)) dz, \quad h_L(t) = \frac{E_c(A_c/2)q_g}{L} \int_0^l (v(z,t) + b\vartheta(z,t)) dz, \tag{10a, b}$$

where E_c is the elastic modulus and A_c is the total cross-sectional area of the main cables, b is the half-width between the main cables, $L = \int_0^l \sqrt{1 + (dy_c/dz)^2} dz$ is the cable length, with good approximation is $L \approx l$ in case of shallow cable ($y_c/l < 1/8$). The self-excited actions of lift and moment, L_{se} and M_{se} , are expressed as follows:

$$L_{se} = \frac{1}{2} \rho U^2 B \left(KH_1^*(K) \frac{\dot{v}}{U} + KH_2^*(K) \frac{B\dot{\vartheta}}{U} + K^2 H_3^*(K) \vartheta + K^2 H_4^*(K) \frac{v}{B} \right), \tag{11}$$

$$M_{se} = \frac{1}{2} \rho U^2 B^2 \left(KA_1^*(K) \frac{\dot{v}}{U} + KA_2^*(K) \frac{B\dot{\vartheta}}{U} + K^2 A_3^*(K) \vartheta + K^2 A_4^*(K) \frac{v}{B} \right), \tag{12}$$

with the same meaning of symbols already introduced in Section 2.1.

Note that Eqs. (9a) and (9b), in addition to the aerodynamic coupling due to the flutter derivatives $H_2^*, H_3^*, A_1^*, A_4^*$ (see Eqs. (11) and (12)), result statically coupled because of the presence of the moment m_y induced by the drag force, which produces the destabilizing second-order effects $(m_y \vartheta)''$ and $m_y v''$. These latter can be responsible of a Prandtl-like lateral-torsional buckling [23],[24]. $m_y = D_s z(l-z)/2$ if the deck-girder is simply supported for horizontal bending, $m_y = D_s [-l^2/12 + z(l-z)/2]$ in case it is doubly clamped (the contribution of the cables is ignored); all the intermediate situations are comprised between the previous two extreme cases. In the analyses conducted in the present study, the bridge deck was considered simply supported at both ends for horizontal bending.

If the terms $(m_y \vartheta)''$ and $m_y v''$ in Eqs. (9a) and (9b) are neglected, one obtains the linearized flutter equations involving vertical bending and torsion [25], the static part of which rests on the well-known linearized deflection theory of the stiffened suspension bridge [25,27,28]. The deflection theory of suspension bridges was originally introduced by Melan in 1888 limited to vertical bending [29], and then extended to bending-torsion behavior by Moisseiff and Lienhard in 1933 [30] and by Bleich in 1935 [31]. To the best of the authors' knowledge, the linearized flutter equations with second-order effects as they appear in Eqs. (9a) and (9b) seem to be original. At the same time, fully geometrically nonlinear formulations of continuum models of suspension bridges, also suitable for flutter and post-flutter analysis, can be found in [25] and in the references contained in it.

The dynamic solution to Eqs. (9a) and (9b) is sought in the form:

$$v(z,t) = \eta(z) e^{i\omega t}, \quad \vartheta(z,t) = \psi(z) e^{i\omega t}, \tag{13a, b}$$

where $\eta(z), \psi(z)$ are the eigenfunctions (vibration modes with no wind) and $\omega_v = \omega_{vr} + i\omega_{vi}$, $\omega_\vartheta = \omega_{\vartheta r} + i\omega_{\vartheta i}$ the corresponding complex eigenvalues. In this case, dynamic instability (i.e. flutter) occurs when the imaginary part of one or more eigenvalues becomes negative, the corresponding real part becoming the flutter frequency ω_f .

A free vibration analysis with no wind, including the effect of the bridge self-weight, must be conducted prior to the flutter analysis. Antisymmetric and symmetric vibration modes are analyzed separately: the former are expressed by sine functions with even number of half-waves (2, 4, 6, ...), while the latter by a series of sine functions with odd number of half-waves (1, 3, 5, ...). The analysis can be extended to the first n eigenfunctions $\eta_j(z), \psi_j(z)$ and corresponding eigenvalues $\omega_{vj} = \omega_{vr,j} + i\omega_{vi,j}$, $\omega_{\vartheta j} = \omega_{\vartheta r,j} + i\omega_{\vartheta i,j}$ ($j=1, 2, 3, \dots, n$). It can be shown that the j^{th} antisymmetric mode is well approximated by a single sine function with a number $2j$ of half-waves ($\sin(2\pi z/l), \sin(4\pi z/l), \sin(6\pi z/l), \dots$) [22]:

$$\eta_j^A(z) = a_{jk} \sin\left(\frac{k\pi z}{l}\right), \quad \text{with } k = 2j, \tag{14a}$$

$$\psi_j^A(z) = b_{jk} \sin\left(\frac{k\pi z}{l}\right), \quad \text{with } k = 2j, \tag{14b}$$

whereas the analysis of the lower symmetric modes requires considering a series expansion with at least four terms for a good approximation (the single term expression gives a good approximation for the higher symmetric modes with $j > 3$, a case in which the magnitude of the incremental tensions h_R, h_L decreases rapidly with an increasing number of half-waves of the vibration mode) [22]. Therefore, for the symmetric modes, we can set in general:



$$\eta_j^s(z) = a_{j1} \sin\left(\frac{\pi z}{l}\right) + a_{j3} \sin\left(\frac{3\pi z}{l}\right) + a_{j5} \sin\left(\frac{5\pi z}{l}\right) + \dots + a_{j(2n-1)} \sin\left(\frac{(2n-1)\pi z}{l}\right), \tag{15a}$$

$$\psi_j^s(z) = b_{j1} \sin\left(\frac{\pi z}{l}\right) + b_{j3} \sin\left(\frac{3\pi z}{l}\right) + b_{j5} \sin\left(\frac{5\pi z}{l}\right) + \dots + b_{j(2n-1)} \sin\left(\frac{(2n-1)\pi z}{l}\right). \tag{15b}$$

Each sine function in Eqs. (14a), (14b) and (15a), (15b) satisfies the same boundary conditions as the functions $\eta(z)$ and $\psi(z)$ (in principle, other suitable functions that satisfy the same boundary conditions can be chosen):

$$\eta(0) = \eta(l) = EI_x \eta''(0) = EI_x \eta''(l) = \psi(0) = \psi(l) = EI_\omega \psi''(0) = EI_\omega \psi''(l) = 0, \tag{16}$$

whereas the parameters a_j and b_j ($j=1, 2, 3, \dots, n$) are to be determined. This can be done by the Ritz energy method [22], based on Hamilton's principle:

$$T - V = \min \tag{17}$$

being T and V the maximum values of the kinetic and potential energy, respectively. Neglecting the mechanical damping (natural vibrations), the difference $T - V$ for the bending and torsion modes in absence of wind can be expressed as follows [22]:

$$T - V = \frac{1}{2} \left[\omega_v^2 \mu_g \int_0^l v^2 dz - EI_x \int_0^l v''^2 dz + H \int_0^l v v'' dz - \frac{E_c A_c}{L} \left(\frac{q_g}{H} \right)^2 \left(\int_0^l v dz \right)^2 \right], \tag{18a}$$

$$T - V = \frac{1}{2} \left[\omega_\theta^2 I_\theta \int_0^l \theta^2 dz - EI_\omega \int_0^l \theta''^2 dz + (GI_t + Hb^2) \int_0^l \theta \theta'' dz - \frac{E_c A_c}{L} \left(\frac{q_g}{H} \right)^2 b^2 \left(\int_0^l \theta dz \right)^2 \right]. \tag{18b}$$

Introducing Eqs. (15a), (15b) into the energy Eqs. (18a), (18b) leads to two expressions showing $T-V$ as quadratic functions of the n parameters a_j or b_j . Thus, setting the minimum condition of Eq. (17) yields, for the symmetric modes:

$$\frac{\partial(T - V)}{\partial a_{j1}} = 0, \quad \frac{\partial(T - V)}{\partial a_{j3}} = 0, \quad \frac{\partial(T - V)}{\partial a_{j5}} = 0, \quad \dots, \quad \frac{\partial(T - V)}{\partial a_{j(2n-1)}} = 0, \tag{19a}$$

$$\frac{\partial(T - V)}{\partial b_{j1}} = 0, \quad \frac{\partial(T - V)}{\partial b_{j3}} = 0, \quad \frac{\partial(T - V)}{\partial b_{j5}} = 0, \quad \dots, \quad \frac{\partial(T - V)}{\partial b_{j(2n-1)}} = 0, \tag{19b}$$

which represent two homogeneous systems of n linear equations in the parameters a_j or b_j . Setting the determinants of the coefficient matrices of Eqs. (19a) and (19b) equal to zero leads to two algebraic equations of the n^{th} degree in the unknowns ω^2 which represent the two frequency equations determining ω_{vj} and $\omega_{\theta j}$. Upon computing the eigenvalues ω_j^2 and introducing them into Eqs. (19a) and (19b), the corresponding values of the parameters a_j and b_j can be computed but for a nonessential multiplicative constant, and the shapes of the symmetric vertical bending and torsional vibration modes can be established (eigenfunctions). It is important to note that in starting from n -term expressions in Eqs. (15a), (15b), the energy method furnishes the first n symmetric bending, torsion modes in one single step. Each frequency equation yields n different roots ω^2 corresponding to the first, second, ..., n^{th} mode of vibration [22]. For example, for $n=5$ one obtains the first five frequencies of symmetric bending and the first five frequencies of symmetric torsion. Introducing Eqs. (14a), (14b) into the energy Eqs. (18a), (18b) and imposing the minimum conditions for the antisymmetric modes analogous to those of Eqs. (19a), (19b) allows determining the first n frequencies of antisymmetric bending and the first n frequencies of antisymmetric torsion.

In suspension bridges, usually the first vibration mode is that of symmetric lateral bending (here to be computed apart), then followed by vertical bending and torsion modes. Among the latter, antisymmetric modes tend to be dominant in suspension bridges with relative short side spans compared to the central span, whereas symmetric vibration modes prevail on antisymmetric ones when the side spans are relatively long. This is because symmetric modes require increments in the cable tension, while antisymmetric modes do not (the integrals in Eqs. (10a, b) identically vanish); therefore, symmetric vibration modes require in general higher energy levels to activate than antisymmetric ones. In addition, the shorter are the side spans, the higher is the effective axial stiffness of the suspension cables in the central span. Of course, the real vibration modes of a suspension bridge are combinations of the aforementioned elementary modes [25]. Such coupling is usually better described by finite element models.

In presence of wind action, an approximate solution to the system defined by Eqs. (9a) and (9b) can be found by applying the Galerkin method [32]. Inserting Eqs. (13a, b) into Eqs. (9a), (9b), with the functions $\eta(z)$ and $\psi(z)$ expressed by Eqs. (14a), (14b) or (15a), (15b), and then imposing the following integral conditions

$$\int_0^l E_1(z, t) \eta_j(z) dz = 0, \quad \int_0^l E_2(z, t) \psi_j(z) dz = 0, \tag{20a, b}$$

yields the following complex eigenvalue problem, of dimension 2×2 :

$$\det \left[-\omega^2 \mathbf{M} + i\omega(\mathbf{C} - \mathbf{C}_{ae}) + (\mathbf{K} - \mathbf{K}_g^D - \mathbf{K}_{ae}) \right] = 0, \tag{21}$$

where \mathbf{K}_g^D is the geometric stiffness matrix associated with the drag-induced second-order effects, i.e. the initial stress matrix due to D_s , the remaining symbols having the same meaning already introduced. From Eq. (21), the values of ω^2 are obtained as functions of (U, U_f) by applying an iterative procedure. As before, a mode-by-mode tracing method must be employed to iteratively look for the flutter critical couple (U_{fj}, ω_j) ; U_{fj} is the reduced flutter velocity, ω_j is the flutter (circular) frequency. Eventually, the flutter wind velocity is thus obtained as $U_f = \omega_f B U_{fj} / 2\pi$. Note that for $U=0$, the natural frequencies of the bridge in absence of wind are recovered.



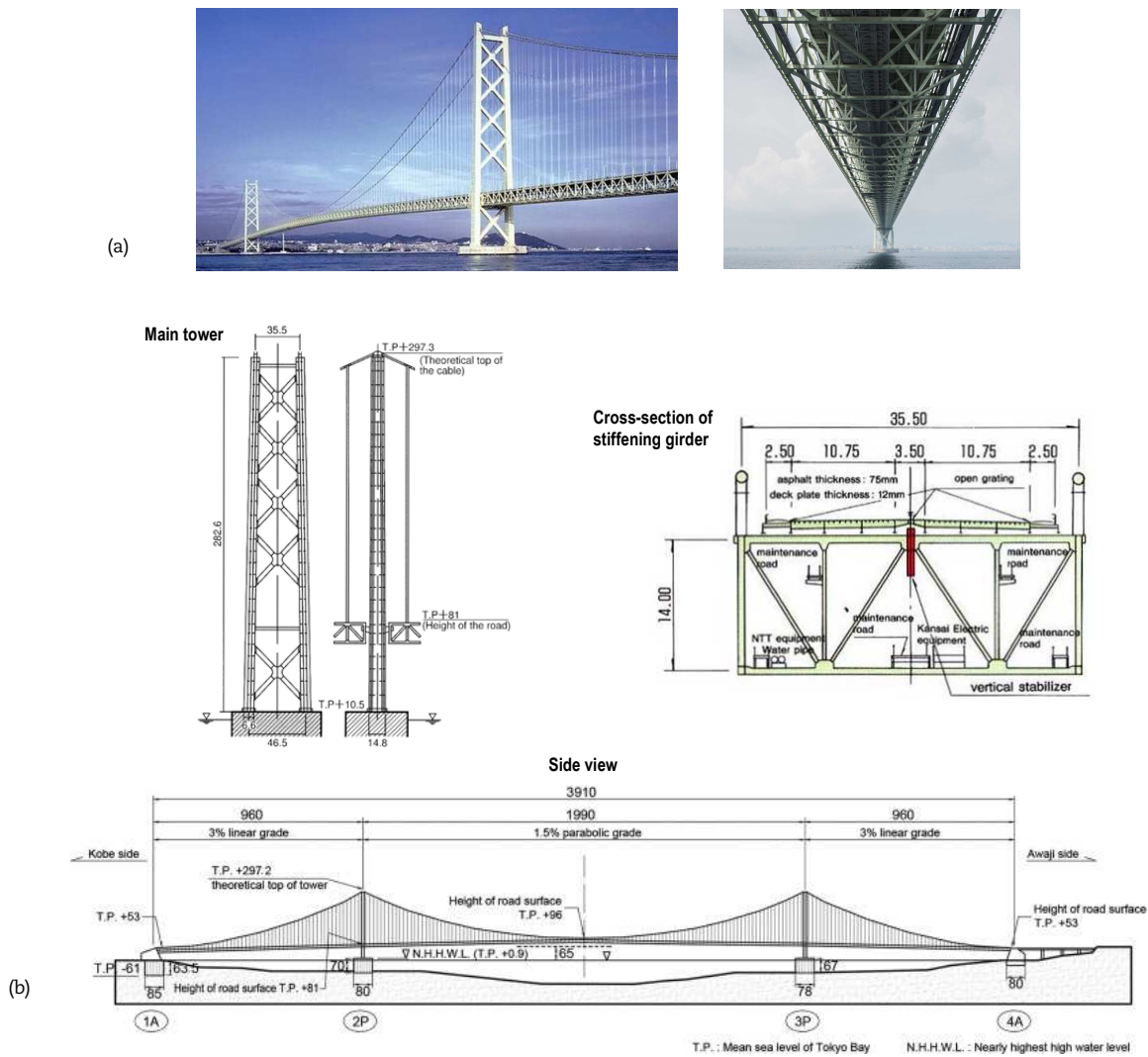


Fig. 2. Layout of Akashi Kaikyo Bridge: (a) global view and bottom view of stiffening girder, (b) main tower, cross-section of stiffening girder and side view (dimensions in m).

According to the procedure described above, Eq. (21) allows studying a bi-modal flutter in which only one vertical bending mode and one torsion mode are involved. It is reasonable to combine the first symmetric bending mode with the first symmetric torsion mode, as well as the first antisymmetric bending mode with the first antisymmetric torsion mode. Of course, other combinations, also involving the higher modes, are possible. In general, the couple of selected modes yielding the lowest flutter velocity will be the critical one. This procedure will be applied in the next section to the selected case study. In general, a multi-mode flutter analysis can be conducted by expressing the functions $v(z,t)$ and $\vartheta(z,t)$ in Eqs. (13a, b) by a weighted series of m eigenmodes ($m \leq n$), each one described by an n -term expression of the type (14a), (14b) or (15a), (15b). In this case, applying the Galerkin method yields a complex eigenvalue problem of dimension $2m \times 2m$, formally identical to that of Eq. (21) [25]. This problem will be dealt with in future contributions.

3. Case Study and Results

Figure 2 shows the general layout of the Akashi Kaikyo Bridge, while the main geometrical and mechanical properties are listed in Tab. 1 [21]. General information on the bridge design and realization can be found in [33]-[35].

A finite element model of the central span was built in ANSYS 15.0 (Fig. 3). BEAM188 finite element was adopted to model main cables and truss girder, whereas LINK180 element was assigned to the hangers [36]. A free vibration analysis without wind action was run in the pre-stressed condition under permanent loads prior to flutter analysis. Table 2 collects the natural vibration frequencies obtained by the FEM model, where they are compared to others available in the literature [21],[37],[38]. In the same table, the frequencies furnished by the semi-analytic model are also reported; see the comments reported below in this section. Figure 4 shows a comparison of the mode shapes obtained in ANSYS and in MATLAB. The first 16 modes are shown: the first four symmetric and the first four antisymmetric modes of vertical bending are in Fig. 4a, whereas the first four symmetric and the first four antisymmetric torsion modes are in Fig. 4b. In the same figure, the modes are identified with respect to those calculated in MATLAB and indicated in Tab. 2 (further comments are reported later on in this section). Table 3 shows the MAC (Modal Assurance Criterion) [39] and NMD (Normalized Modal Difference) [40] indices, used here to evaluate the correlation between a mode shape calculated in ANSYS and the corresponding one obtained in MATLAB. In general, MAC and NMD are defined as follows:



Table 1. Main geometrical and mechanical properties of the Akashi Kaikyo Bridge.

Property	Measure	Property	Measure
Central span length (m)	1,991	Diameter of hangers (m)	0.19
Side spans length (m)	960	Inertia moment for vertical bending (m ⁴)	24
Towers height (m)	282.6	Inertia moment for lateral bending (m ⁴)	130
Truss girder width (m)	35.5	Inertia moment for torsion (m ⁴)	17.8
Truss girder depth (m)	14	Deck-girder mass (t/m)	28.7
Cross-section of each main cable (m ²)	0.79	Polar inertia moment of girder (t m ² /m)	5,800

Table 2. Natural vibration frequencies (in Hz) of Akashi Kaikyo Bridge from present study and literature ($\Delta=(f_{MAT} - f_{ANS}) / f_{ANS} \times 100$).

Mode ⁽¹⁾	ANSYS, f_{ANS}	MATLAB, f_{MAT}	Δ (%)	Jurado et al. [21]	Katsuchi [37]	Miyata et al. [38]
LS	0.0371	-	-	0.0451	0.0388	0.0387
VS	0.0602	0.0618 (VS1)	2.7	0.0662	0.0652	0.0638
VA	-	-	-	0.0736	0.0753	0.0745
VA	0.0829	0.0769 (VA1)	-7.2	0.0850	0.0850	0.0835
LA	0.0719	-	-	0.0946	0.0783	0.0775
VS	0.1222	0.1204 (VS2)	-1.4	0.1227	0.1217	0.1213
LTS	0.1193	-	-	0.1581	0.1271	0.1497
VS	-	-	-	0.1623	0.1638	-
TLS	0.1311	0.1301 (TS1)	-0.7	0.1635	0.1551	-
VA	0.1662	0.1653 (VA2)	-0.5	0.1741	0.1714	-
LTA	0.2087	-	-	0.2196	0.2114	0.2077
VS	0.2181	0.2171 (VS3)	-0.5	0.2270	0.2212	-
TLA	0.2241	0.2289 (TA1)	2.1	0.2390	0.2547	-
LA	-	-	-	0.2504	0.2212	-
LTS	-	-	-	0.2610	0.2970	-
VA	0.2751	0.2746 (VA3)	-0.2	0.2819	-	-
TLS	0.3353	0.3440 (TS2)	2.6	0.3210	-	-
VS	0.3393	0.3390 (VS4)	-0.1	-	-	-
VA	0.4120	0.4106 (VA4)	-0.3	-	-	-
LTA	0.4498	-	-	-	-	-
TLA	0.4548	-	-	-	-	-
TA	0.4570	0.4578 (TA2)	0.2	-	-	-
VS	0.4893	-	-	-	-	-
TS	0.5560	0.5724 (TS3)	2.9	-	-	-
TA	0.6699	0.6867 (TA3)	2.5	-	-	-
TS	0.7826	0.8012 (TS4)	2.4	-	-	-
TA	0.8900	0.9156 (TA4)	2.9	-	-	-

⁽¹⁾ L = lateral, V= vertical, T = torsional, S = symmetric, A = antisymmetric (lateral deformation not included in MATLAB model)

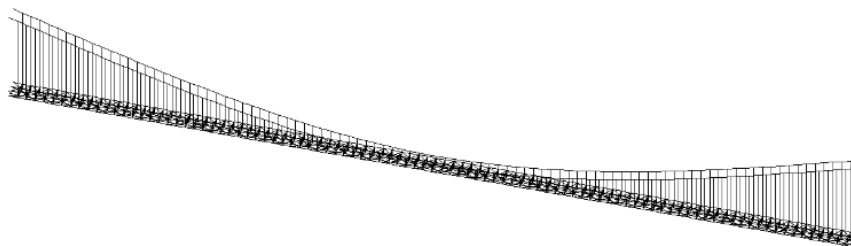


Fig. 3. FEM model of the central span built in ANSYS 15.0.

$$MAC(\varphi_{A,k}, \varphi_{B,j}) = \frac{(\varphi_{A,k}^T \varphi_{B,j})^2}{(\varphi_{A,k}^T \varphi_{A,k})(\varphi_{B,j}^T \varphi_{B,j})}, \quad NMD(\varphi_{A,k}, \varphi_{B,j}) = \sqrt{\frac{1 - MAC(\varphi_{A,k}, \varphi_{B,j})}{MAC(\varphi_{A,k}, \varphi_{B,j})}}, \quad (22a, b)$$

with $\varphi_{A,k}$ the k -th mode of the data set A and $\varphi_{B,j}$ the j -th mode of the data set B (values in Tab. 3 were calculated with $k=j$ to compare homologous modes). MAC is analogous to the correlation coefficient in statistics and is unaffected by the individual scaling of mode vectors. MAC ranges [0,1]: 1 implies a perfect correlation of the two mode vectors, while 0 indicates uncorrelated (i.e., orthogonal) vectors. NMD is a close estimate of the average difference between the components of the vectors $\varphi_{A,k}$ and $\varphi_{B,j}$; e.g., if MAC equals 0.950, then NMD is 0.2294, meaning that the components of $\varphi_{A,k}$ and $\varphi_{B,j}$ differ 22.94% average. Usually, $MAC > 0.80$ implies a good match, while $MAC < 0.40$ indicates a poor match. NMD is much more sensitive to mode shape differences than the MAC and hence is introduced to highlight the differences between highly correlated mode shapes. The values in Tab. 3 show an almost perfect correlation among ANSYS and MATLAB mode vectors (the NMD values shown were obtained from MAC values having 15 digits after the decimal point, and not using the approximated values shown in Tab. 3).



Table 3. MAC and NMD correlation indices for ANSYS vs. MATLAB mode shapes in Fig. 4.

Mode	MAC	NMD	Mode	MAC	NMD
VS1	0.9959	0.0639	TS1	1.0000	0.0025
VA1	0.9998	0.0123	TA1	0.9998	0.0123
VS2	0.9928	0.0850	TS2	0.9994	0.0250
VA2	0.9977	0.0477	TA2	0.9977	0.0477
VS3	0.9927	0.0860	TS3	0.9935	0.0806
VA3	0.9950	0.0711	TA3	0.9950	0.0711
VS4	0.9945	0.0745	TS4	0.9945	0.0742
VA4	0.9884	0.1083	TA4	0.9884	0.1083

The flutter derivatives of interest, necessary to define the aerodynamic stiffness and damping matrices through the Matrix27 element, were taken from Katsuchi et al. [41]. They are shown in Fig. 5 and correspond to the cross-section modified by inserting a vertical stabilizer (see Fig. 2) to improve the aerodynamic behavior of the bridge [41].

Figure 6 shows the results of flutter analysis in cases 1, 2 and 3. Real and imaginary parts of complex eigenvalues λ are shown in the left and right panels, respectively. The eigenvalues of the fundamental symmetric and antisymmetric modes of vertical bending and torsion are plotted against the wind velocity U . Flutter velocity and frequency are respectively equal to 81.3 m/s and 0.122 Hz in case 1 (Fig. 6a), 76.4 m/s and 0.131 Hz in case 2 (Fig. 6b), whereas no flutter was detected within the 0-100 m/s wind speed range in case 3 (Fig. 6c). The mode-by-mode tracing method adopted here identified the first symmetric torsion mode as the one responsible for flutter (see Fig. 6a, b). This result is coherent with those of multi-mode flutter analyses, which have found the flutter of the Akashi- Kaikyo Bridge to be a multi-mode coupled flutter where the first mode of symmetric torsion is the primary flutter mode [41].

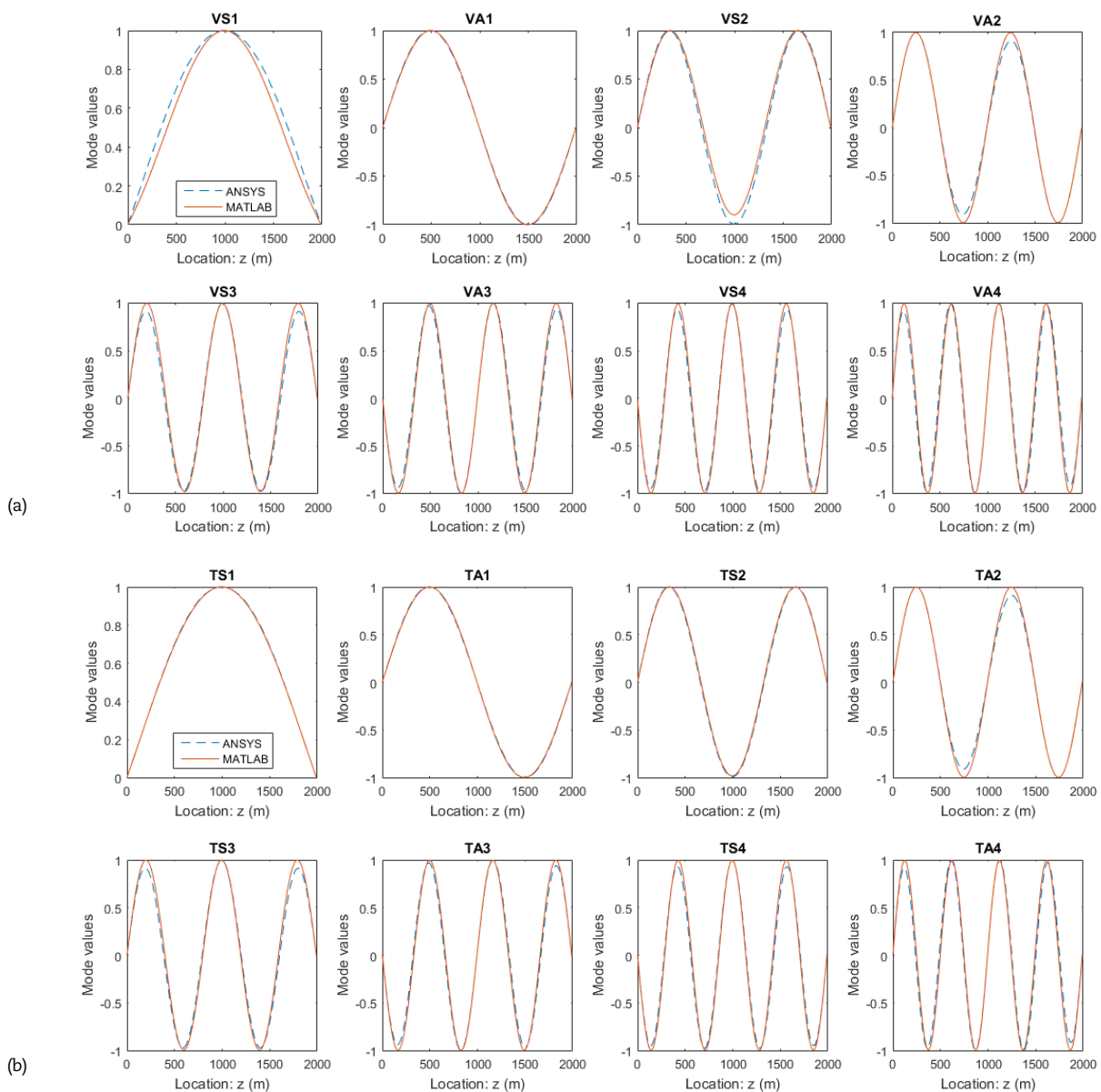


Fig. 4. Comparison among (a) vertical and (b) torsion mode shapes obtained in ANSYS and in MATLAB: the modes shown are those identified in Tab. 2.



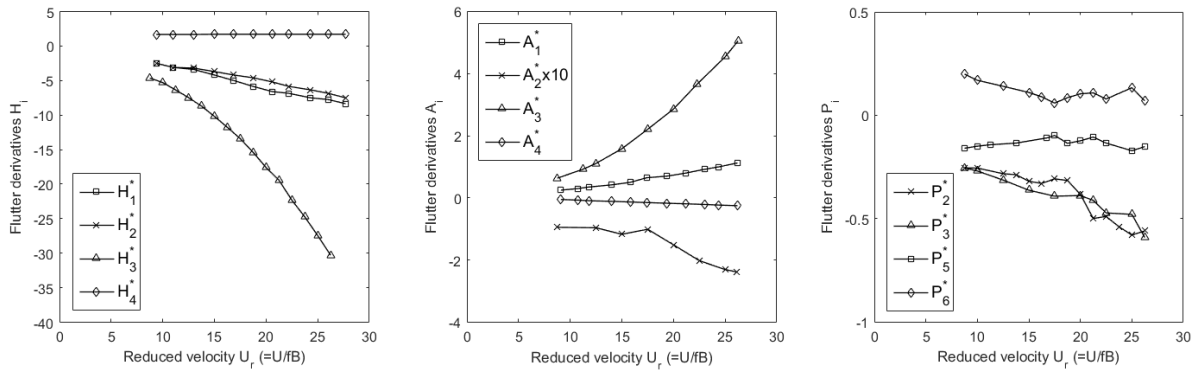


Fig. 5. Flutter derivatives used in flutter analyses (modified cross section, no cables, $\alpha = 0^\circ$) [41].

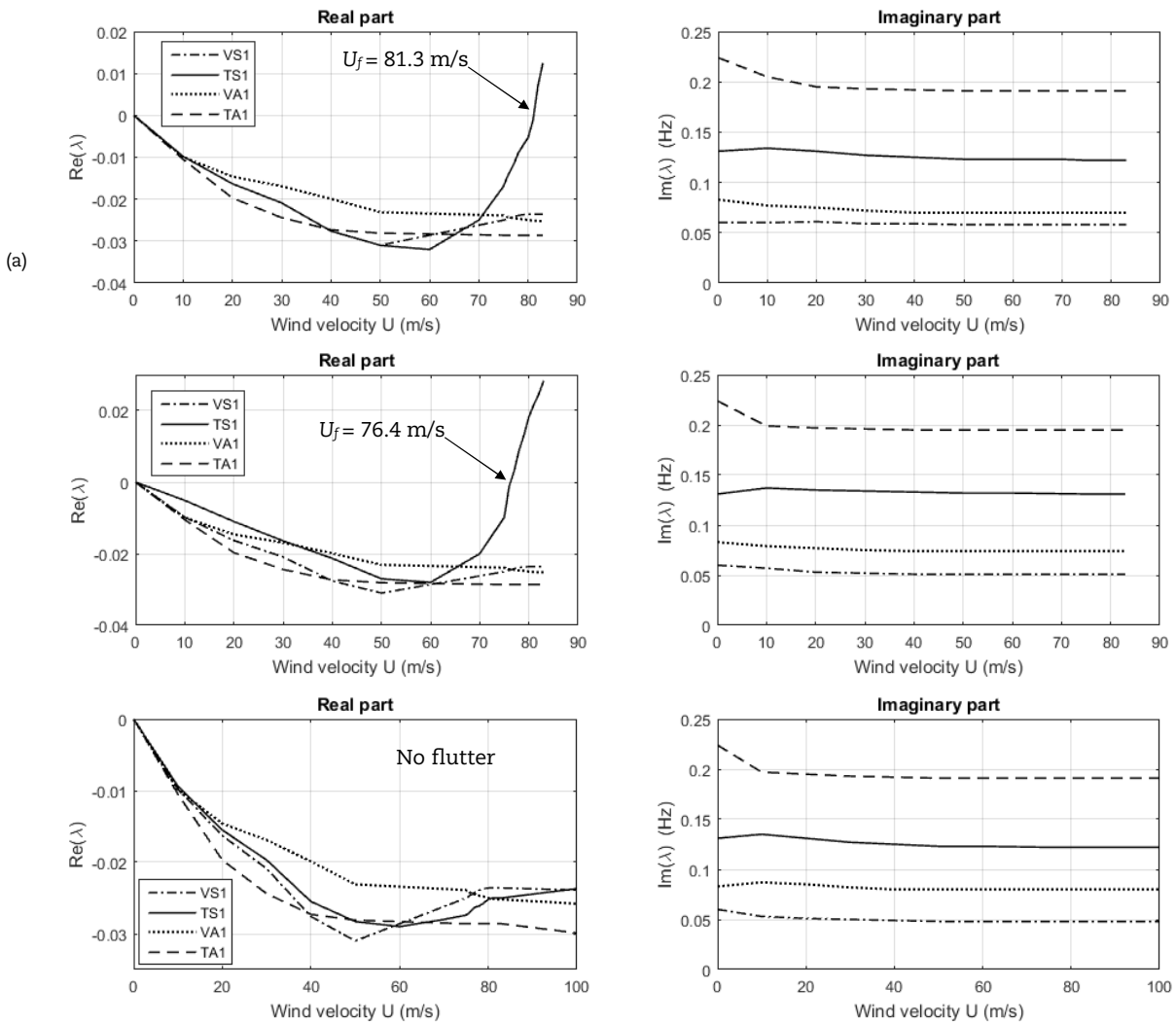


Fig. 6. Real and imaginary parts of complex eigenvalues λ from FEM flutter analysis in (a) case 1, (b) case 2 and (c) case 3.

Table 4. Input parameters adopted for the continuum model of the Akashi Kaikyo Bridge.

Property	Measure	Property	Measure
l (m)	1,991	I_s (kg m ² /m)	8.33E+06
f (m)	219	q_g (N/m)	403,378
E (N/m ²)	2.10E+11	E_c (N/m ²)	1.60E+10
G (N/m ²)	8.10E+10	A_c (m ²)	1.58
B (m)	35.5	b (m)	17.75
I_x (m ⁴)	24	ρ (kg/m ³)	1.25
I_w (m ⁶)	0	$C_D(0)$ (/)	0.386
I_t (m ⁴)	17.8	ζ_w (%)	0.485
μ_g (kg/m)	41,119	ζ_g (%)	0.653



Table 5. Comparison among flutter velocity and flutter frequency from FEM, continuum model and literature.

Flutter velocity Flutter frequency	Literature [41] [ⓐ] Calculated; Measured	FEM ($L_{se}+M_{se}+D_{se}$)	FEM ($L_{se}+M_{se}+D_s$)	FEM ($L_{se}+M_{se}$)	Continuum model ($L_{se}+M_{se}+D_s$)
U_f (m/s)	81.3; 90.0	81.3 ($\Delta = 0\%$; -9.7%)	76.4 ($\Delta = -6.0\%$; -15.1)	-	80.1 ($\Delta = -1.5\%$; -11.0%)
$\omega_f/2\pi$ (Hz)	0.148; 0.140	0.122 ($\Delta = -17.6\%$; -12.9%)	0.131 ($\Delta = -11.5\%$; -6.4%)	-	0.098 ($\Delta = -33.8\%$; -30.0%)

[ⓐ] Modified cross section, $\alpha = 0^\circ$. For original cross section, $\alpha = 0^\circ$: $U_f = 79.1$ m/s (calculated), 84.0 m/s (measured); $\omega_f/2\pi = 0.146$ Hz (calculated), 0.135 Hz (measured)

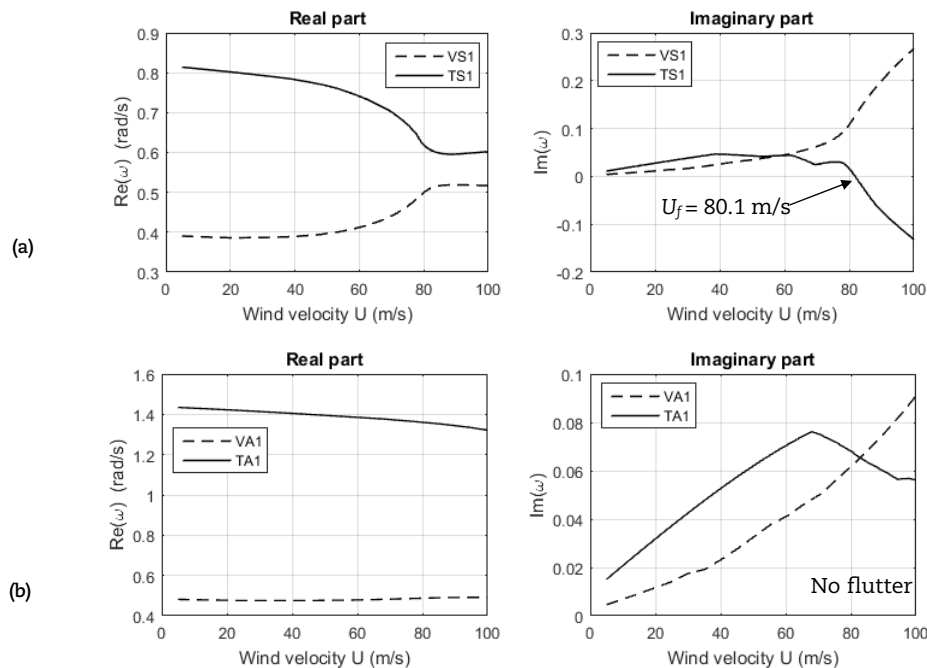


Fig. 7. Real and imaginary parts of complex eigenvalues ω from continuum model for (a) fundamental symmetric and (b) fundamental antisymmetric modes.

Table 4 lists the input parameters adopted for the analysis of the Akashi Kaikyo Bridge by means of the semi-analytic continuum model. A free vibration analysis without wind (under the effect of the bridge self-weight) was conducted prior to the flutter analysis. The symmetric modes of vertical bending and torsion were analyzed by adopting a series of 10 sine functions (i.e., $n=10$) in Eqs. (15a) and (15b), respectively; therefore, the first 10 symmetric bending modes and the first 10 symmetric torsion modes, and corresponding frequencies, were obtained. The first 10 antisymmetric bending and torsion frequencies were obtained starting from the modes defined by Eqs. (14a) and (14b). The results for the first 4 modes of symmetric bending, symmetric torsion, antisymmetric bending, and antisymmetric torsion, for a total of 16 modes, are collected in Tab. 2 (natural frequencies) and in Fig. 4, Tab. 3 (vibration modes), where they are compared to the FEM results.

The flutter derivatives of interest are the H_i and A_i reported in Fig. 5. The numerical solution to Eq. (21) was obtained by a self-built MATLAB script. The fundamental modes of symmetric bending and torsion were analyzed together, as well as the antisymmetric bending and torsion modes. The results of the two flutter analyses are shown in Figs. 7a and 7b for the symmetric and antisymmetric modes, respectively. As before, the mode responsible for flutter instability is the first of symmetric torsion. The critical condition is identified by $U_f = 80.13$ m/s, $\omega_f = 0.616$ rad/s ($=0.098$ Hz); the corresponding reduced flutter velocity is $U_{f,r} = 23.03$. Jurado et al. [21], by a bi-modal flutter analysis involving the first symmetric bending mode ($f = 0.0662$ Hz; see Tab. 2 or [21]) and the first symmetric torsion mode ($f = 0.1635$ Hz; see Tab. 2 or [21]) obtained a flutter velocity $U_f = 77.69$ m/s and a flutter frequency of $\omega_f = 0.997$ rad/s ($=0.159$ Hz), the critical flutter mode being the torsion mode. Note that the percentage differences between the present MATLAB predictions and the corresponding values of Jurado et al. [21] are -6.6% for the bending frequency (0.0618 vs. 0.0662 Hz) and -20.4% for the torsion frequency (0.1301 vs. 0.1635 Hz); see Tab. 2. This partially explains the -38.4% difference in the predicted flutter frequencies (0.098 vs. 0.159 Hz). The same authors, by a multi-mode flutter analysis involving 17 modes, obtained $U_f = 93.33$ m/s, $\omega_f = 1.33-0.95$ rad/s ($=0.21-0.15$ Hz) [21].

Table 5 collects the results in terms of flutter velocity and frequency given by the FEM analyses and by the continuum model, compared to calculated and measured values from literature [41]. In the same table, percentage differences between the present study and the literature values are indicated by Δ . We see that, with respect to the selected reference values, the flutter velocity was underestimated by 0–15% about by the FEM analyses and by 1.5–11% by the continuum model. The flutter frequency was underestimated by 6.4–17.6% by the FEM analyses and by 30% about by the continuum model. No flutter was predicted in the 0–100 m/s wind velocity range by the FEM analysis that did not include the drag force. The prediction of the flutter frequency of both FEM and continuum models is susceptible of refinement. A model updating devoted to reduce the differences among the natural frequencies predicted in the present study and those of the literature should help in this sense (see Tab. 2).



4. Conclusion

In this paper, we investigated the influence of the drag force and of its description on the flutter velocity and frequency of the Akashi Kaikyo Bridge. For this purpose, we compared results available in the literature with those obtained in the present study by a finite element analysis and by an *in-house* MATLAB code based on a semi-analytic continuum model. The latter is proposed by the authors to enhance existing linearized continuum models for the flutter analysis of suspension bridges by including the destabilizing effect of the drag force as a Prandtl-like second-order contribution. A detailed finite element model of the central span was built in ANSYS, and flutter analyses were run according to the following three descriptions of the aerodynamic loads: (1) unsteady lift, moment and drag; (2) unsteady lift and moment, plus steady drag; and (3) unsteady lift and moment, without drag. The unsteady (self-excited) forces were described, by means of user-defined Matrix27 finite elements suitably attached to the bridge deck [16], in terms of aerodynamic stiffness and damping matrices based on the bridge's flutter derivatives taken from the literature [41]. As for the *in-house* code, the flutter analysis is based on a semi-analytic continuum model of the bridge's central span that includes flexural-torsional second-order effects induced by the steady drag force into the equations of motion, in addition to the unsteady actions of lift and moment. For both the FEM and the semi-analytic approach, after a preliminary free-vibration analysis without wind, dynamic stability was analyzed as a complex eigenvalue problem, where a mode-by-mode tracing method was employed to iteratively search for flutter critical condition.

For the analyzed case, with respect to literature results, the analyses confirm that including the drag force is, in facts, necessary to correctly estimate the flutter velocity, but also indicate that good predictions can be obtained by combining steady drag together with unsteady lift and moment, provided the geometric nonlinearity in the deck and main cables is taken into account. In particular, both the FEM and semi-analytic approaches gave good (and conservative) predictions in terms of flutter speed. The latter was underestimated by 0–15% about by the FEM analyses and by 1.5–11% by the continuum model. The adopted procedures identified the first symmetric torsion mode as the one responsible for flutter onset, a result which is in line with others of literature (e.g., see [41]). The corresponding flutter frequency was underestimated by 6.4–17.6% by the FEM analyses and by 30% about by the continuum model. A refinement in the flutter velocity and frequency predicted this time by the semi-analytic approach with respect to those reported in [19] was possible thanks to an improved description of the symmetric torsion vibration modes and frequencies. In fact, whilst in [19] the same spatial functions adopted for describing the symmetric bending modes were employed also for the description of the symmetric torsion modes, in the present study the two sets of functions were obtained independently (see Section 2.3). Nevertheless, the prediction is still susceptible of further improvement, e.g. through a model updating. In general, from the satisfactory comparisons among the literature results and the predictions obtained here, we deduce that the simplifying assumptions made in this study are quite acceptable.

The FEM approach results to be more accurate, but also more time consuming, than the semi-analytic one, which, however, can conveniently be used for rapid or preliminary calculations. In the present study, the proposed semi-analytic continuum model was used to conduct a bi-modal flutter analysis. Application to multi-mode flutter analysis will be presented in future contributions.

Author Contributions

GP and AC conceived the study. GP performed the analyses and wrote the paper. GP and AC discussed the results, reviewed, and approved the final version of the manuscript.

Acknowledgments

The authors gratefully acknowledge the help of Eng. Sebastiano Russo in some numerical calculations.

Conflict of Interest

The authors declared no potential conflicts of interest with respect to the research, authorship, and publication of this article.

Funding

The authors received no financial support for the research, authorship, and publication of this article.

Nomenclature

a_j, b_j	Parameters of mode shape functions ($j=1, 2, \dots, n$) [1]	m_y	Bending moment due to drag force D_s [N m]
A_c	Total cross-section area of main cables [m ²]	$\mathbf{M}, \mathbf{C}, \mathbf{K}$	Global mass, damping, stiffness matrices
b	Half-distance between main cables [m]	M_{se}	Self-excited moment per unit length [N m/m]
B	Deck width [m]	q_g	Total bridge weight per unit length (N/m)
$\mathbf{C}_{ae}, \mathbf{K}_{ae}$	Global aerodynamic damping, stiffness matrices	t	Time coordinate [s]
$\mathbf{C}_{ae}^e, \mathbf{K}_{ae}^e$	Aerodynamic damping, stiffness matrices of element e	T, V	Maximum values of kinetic, potential energy [J]
C_D	Drag coefficient [1]	U	Wind velocity [m/s]
c_v	Vertical damping coefficient [N s/m]	U_f	Flutter (wind) velocity [m/s]
c_g	Torsion damping coefficient [N m s/m]	U_r	Reduced (wind) velocity [1], $2\pi/K$
D_s	Steady drag force per unit length [N/m]	U_{rf}	Reduced flutter velocity [1]
D_{se}, L_{se}	Self-excited drag, lift forces per unit length [N/m]	$v(z,t)$	Vertical deflection of deck [m]
E	Young's modulus of deck [N/m ²]	$v_l(t), v_r(t)$	Vertical deflection of left, right main cables [m]
E_c	Elastic modulus of main cables [N/m ²]	$y_c(z)$	Initial parabolic profile of main cables [m]
f	Cables sag [m]	x, y, z	Spatial coordinates (z =axial one along deck axis) [m]
G	Shear modulus of deck [N/m ²]	\mathbf{x}	Complex eigenvector
$h(t), p(t)$	Vertical, lateral displacements of deck section [m]	\mathbf{X}	Dynamic response vector
$h_r(t), h_l(t)$	Additional horizontal force in right, left cables [N]	$\alpha(t)$	Torsional rotation of deck (wind attack angle) [1]
H	Total horizontal force in main cables [N]	ζ_v, ζ_g	Bending, torsion damping ratios [1]





H_i^*, P_i^*, A_i^*	Flutter derivatives ($i=1, 2, \dots, 6$) [1]	$\eta(z)$	Mode shape of vertical bending [m]
I_x	Deck moment of inertia for vertical bending [m ⁴]	$\theta(z,t)$	Torsion rotation of deck (=twist angle) [1]
I_t	Deck primary (St. Venant) torsion constant [m ⁴]	λ	Complex eigenvalue
I_ρ	Deck mass polar moment of inertia/unit length [kg m ² /m]	λ_f	(Flutter) critical complex eigenvalue
I_ω	Deck warping constant [m ⁶]	μ_g	Total bridge mass per unit length (kg/m)
K	Reduced frequency [1], $\omega B/U$	ρ	Air mass density [kg/m ³]
\mathbf{K}_g^D	Geometric stiffness matrix of deck	$\Phi_{A,j}, \Phi_{B,j}$	Generic mode shape vectors
l	Length of bridge central span [m]	$\psi(z)$	Torsion mode shape [1]
L	Length of main cables [m]	ω	Circular frequency [rad/s]
L_e	Length of element e [m]	ω_f	(Circular) flutter frequency [rad/s]

References

- [1] Scott, R., *In the Wake of Tacoma: Suspension Bridges and the Quest for Aerodynamic Stability*, ASCE, Reston, 2001.
- [2] Astiz, M.A., Flutter stability of very long suspension bridges, *Journal of Bridge Engineering*, 3(3), 1998, 132-139.
- [3] Scanlan, R.H. Tomko, J.J., Airfoil and Bridge Deck Flutter Derivatives, *Journal of the Engineering Mechanics Division*, 97(6), 1971, 1717-1737.
- [4] Scanlan, R.H., The action of flexible bridges under winds, I: flutter theory, *Journal of Sound and Vibration*, 60(2), 1978, 187-199.
- [5] Scanlan, R.H., Developments in aeroelasticity for the design of long-span bridges, in Miyata T. et al. eds., *Long-Span Bridges and Aerodynamics, Proceedings of the International Seminar Bridge Aerodynamics Perspective*, Kobe, March 1998, Springer, Tokyo, 1999.
- [6] Chen, X., Kareem, A., Matsumoto, M., Multimode coupled flutter and buffeting analysis of long span bridges, *Journal of Wind Engineering and Industrial Aerodynamics*, 89(7-8), 2001, 649-664.
- [7] Wu, B., et al., Characterization of vibration amplitude of nonlinear bridge flutter from section model test to full bridge estimation, *Journal of Wind Engineering and Industrial Aerodynamics*, 197, 2020, 104048.
- [8] Albrecht, P., Namini, A., Bosch, H., Finite Element-Based Flutter Analysis of Cable-Suspended Bridges, *Journal of Structural Engineering*, 118(6), 1992, 1509-1526.
- [9] Salvatori, L., Borri, C., Frequency- and time-domain methods for the numerical modeling of full-bridge aeroelasticity, *Computers & Structures*, 85, 2007, 675-687.
- [10] Zahlten, W., Eusani, R., Numerical simulation of the aeroelastic response of bridge structures including instabilities, *Journal of Wind Engineering and Industrial Aerodynamics*, 94, 2006, 909-922.
- [11] Miata, T., Historical view of long-span bridge aerodynamics, *Journal of Wind Engineering and Industrial Aerodynamics*, 91(12-15), 2003, 1393-1410.
- [12] Abbas, T., Kavrov, I., Morgenthal, G., Methods for flutter stability analysis of long-span bridges: a review, *Proceedings of the Institution of Civil Engineers - Bridge Engineering*, 170(4), 2017, 271-310.
- [13] Miyata, T., et al., New findings of coupled-flutter in full model wind tunnel tests on the Akashi Kaikyo Br., *Proceedings of the International Conference on Cable-Stayed and Suspension Bridges*, Vol. 2, Deauville, France, 1994.
- [14] Zhang, X., Brownjohn, J.M.W., Some considerations on the effects of the P-derivatives on bridge deck flutter, *Journal of Sound and Vibration*, 283(3-5), 2005, 957-969.
- [15] Bartoli, G., Mannini, C., A simplified approach to bridge deck flutter, *Journal of Wind Engineering and Industrial Aerodynamics*, 96(2), 2008, 229-256.
- [16] Hua, X.G., et al., Flutter analysis of long-span bridges using ANSYS, *Wind and Structures*, 10(1), 2007, 61-82.
- [17] Hua, X.G., Chen, Z.Q., Full-order and multimode flutter analysis using ANSYS, *Finite Elements in Analysis and Design*, 44(9-10), 2008, 537-551.
- [18] Chen, G.F., et al., Discussion on "Full-order and multimode flutter analysis using ANSYS" [Finite elements in analysis and design 44(9-10) (2008) 537-551], *Finite Elements in Analysis and Design*, 47(2), 2011, 208-210.
- [19] Piana, G., Carpinteri, A., On the Influence of Drag Force Modeling in Long-Span Suspension Bridge Flutter Analysis, Garcaterra A. et al. eds., *Proceedings of XXIV AIMETA Conference 2019. AIMETA 2019. Lecture Notes in Mechanical Engineering*, Springer, Cham, 2020, 1387-1396.
- [20] Simiu, E., Yeo, D., *Wind Effects on Structures: Modern Structural Design for Wind*, 4th Edition, Wiley, 2019.
- [21] Jurado, J.A., et al., *Bridge Aeroelasticity: Sensitivity Analysis and Optimal Design*, WIT Press, 2011.
- [22] Bleich, F., et al., *The mathematical theory of vibration in suspension bridges*. Department of Commerce, Bureau of Public Roads, Washington, D.C., 1950.
- [23] Como, M., Stabilità aerodinamica dei ponti di grande luce, in Giangreco E. ed., *Ingegneria delle Strutture*, Vol. II, Ch. VII, UTET, Torino, 2002.
- [24] Piana, G., et al., Natural Frequencies of Long-Span Suspension Bridges Subjected to Aerodynamic Loads, *Dynamics of Civil Structures, Volume 4: Proceedings of the 32nd IMAC*, Springer, 2014, 419-431.
- [25] Lacarbonara, W., *Nonlinear Structural Mechanics: Theory, Dynamical Phenomena and Modeling*, Springer, 2013, Ch. 9.
- [26] von Kármán, T., Biot, M.A., *Mathematical Methods in Engineering*, McGraw-Hill, 1940, 277-283.
- [27] Timoshenko, S.P., Young, D.H., *Theory of Structures*, 2nd Edition, McGraw-Hill, 1965, Ch. 11.
- [28] Pugsley, A., *The Theory of Suspension Bridges*, 2nd Edition, Edward Arnold Ltd., London, 1968.
- [29] Melan, J., *Theorie der eisernen Bogenbrücken und der Hängebrücken*, *Handbuch der Ingenieurwissenschaften*, 2, Wilhelm Engelmann, Leipzig, 1888.
- [30] Moisseiff, L.S., Lienhard, F., Suspension Bridges under the Action of Lateral Forces, *Transactions of the American Society of Civil Engineers*, 98(2), 1933.
- [31] Bleich, H.H., *Die Berechnung verankerter Hängebrücken*, Springer, Vienna, 1935.
- [32] Bathe, K.J., *Finite element procedures in engineering analysis*, Prentice-Hall, Englewood Cliff, 1982.
- [33] Kitagawa, M., Technology of the Akashi Kaikyo Bridge, *Structural Control and Health Monitoring*, 11, 2004, 75-90.
- [34] Yim, W.T., Akashi Bridge, *Proceedings of Bridge Engineering 2 Conference 2007*, 27 April 2007, University of Bath, Bath, UK, 2007.
- [35] Pipinato, A., Case study: the Akashi-Kaikyo bridge, in *Innovative Bridge Design Handbook, Construction, Rehabilitation and Maintenance*, Ch. 26, Butterworth Heinemann, 681-699, 2016.
- [36] ANSYS APDL User's Guide, Release 15.0, November 2013, ANSYS, Inc.
- [37] Katsuchi, T., *An Analytical Study on Flutter and Buffeting of the Akashi-Kaikyo Bridge*, Essay submitted in conformity with the requirements for Master of Science in Engineering, 1997.
- [38] Miyata, T., et al., Wind effects and full model wind tunnel tests, *Proceedings of the First International Symposium on Aerodynamics of Large Bridges*, Balkema, Copenhagen, Denmark, 1992, 217-236.
- [39] Allemang, R.J., Brown, D.L., A Correlation Coefficient for Modal Vector Analysis, *Proceedings of the 1st IMAC*, Orlando, Florida, 1982.
- [40] Maya, N.M.M., Silva J.M.M., eds., *Theoretical and experimental modal analysis*, Research Studies Press, Taunton, 1997.
- [41] Katsuchi, H., et al., Multi-mode flutter and buffeting analysis of the Akashi-Kaikyo bridge, *Journal of Wind Engineering and Industrial Aerodynamics*, 77-78(1), 1998, 431-441.

ORCID iD

Gianfranco Piana  <https://orcid.org/0000-0002-3462-0203>

Alberto Carpinteri  <https://orcid.org/0000-0002-5367-6560>



© 2021 Shahid Chamran University of Ahvaz, Ahvaz, Iran. This article is an open access article distributed under the terms and conditions of the Creative Commons Attribution-NonCommercial 4.0 International (CC BY-NC 4.0 license) (<http://creativecommons.org/licenses/by-nc/4.0/>).



How to cite this article: Piana G., Carpinteri A. Long-span Suspension Bridge Flutter Analysis with Drag Force Effects, *J. Appl. Comput. Mech.*, 7(SI), 2021, 1077–1089. <https://doi.org/10.22055/JACM.2021.32481.2025>

Publisher's Note Shahid Chamran University of Ahvaz remains neutral with regard to jurisdictional claims in published maps and institutional affiliations.

